ADVANCED MATERIALS
www.advmat.de

Tuning the Dynamics of Viral-Factories-Inspired Compartments Formed by Peptide–RNA Liquid–Liquid Phase Separation

*Itai Katzir, Elvira Haimov, and Ayala Lampel**

Viral factories are intracellular microcompartments formed by mammalian viruses in their host cells, and contain necessary machinery for viral genome replication, capsid assembly, and maturation, thus serving as "factories" for formation of new viral particles. Recent evidence suggests that these compartments are formed by liquid–liquid phase separation (LLPS) of viral proteins and nucleic acids and present dynamic properties. In this work, inspired by the remarkable functionalities of viral factories, dynamic compartments that are formed by complexation between a minimalistic, disordered peptide and RNA are designed. By systematic studies using sequence variants it is shown that the material properties of the compartments can be modulated by changes to the peptide sequence, at the single amino acid level. Moreover, by taking this approach to the next step, liquid compartments with light-induced tunable dynamics are developed. The results demonstrate that the material properties of liquid droplets can be temporally regulated by increasing peptide polarity and charge, and that these changes can be further utilized for controlled partitioning and release of payloads from the compartments.

1. Introduction

Viral factories are membraneless intracellular compartments formed during the infection of various RNA viruses, including rabies,[1,2] measles,[3–5] and SARS-CoV-2.[6,7] These compartments concentrate proteomic and genomic viral material and compartmentalize the replication and assembly of new viral particles.[1–3,6] Recent studies suggest that viral factories, similar to other intracellular membraneless compartments[8] including stress granules, nucleoli, and Cajal bodies,[9–11] are dynamic and disordered, rather than solid hierarchical assemblies, that are formed by liquid–liquid phase separation (LLPS) of viral proteins and nucleic acids.[1–7,12–14] Specifically, disordered regions[3,6,12,13] within specific viral proteins play a role in complex coacervation and LLPS, where electrostatic interactions are thought to be the main driving force.[13,14] Yet, the exact mechanism of viral factories formation and the underlying network of intermolecular interactions vary between different viral strains and are still not fully understood.

Inspired by the dynamic nature of viral factories which allows partitioned molecules and their protein building blocks to exchange with the surrounding environment and at the same time compartmentalize and regulate complex processes, we developed liquid compartments that can efficiently encapsulate and release payloads. Recently, a number of compartmentalization systems were reported based on LLPS of intrinsically disordered proteins (IDPs).[15,16] These assemblies mimic the properties of membraneless organelles and can compartmentalize and control biocatalytic processes.[17] Yet, their construction involves a complex series of expression and purification steps, which produce limited yields and the control over their physical and material properties remains a challenge. To address these limitations, we utilized a minimalistic approach and developed compartments that are formed by LLPS of a short peptide and RNA.

I. Katzir, A. Lampel
Shmunis School of Biomedicine and Cancer Research
George S. Wise Faculty of Life Sciences
Tel Aviv University
Tel Aviv 69978, Israel
E-mail: ayalalampel@tauex.tau.ac.il

The ORCID identification number(s) for the author(s) of this article can be found under https://doi.org/10.1002/adma.202206371.

DOI: 10.1002/adma.202206371

E. Haimov
Blavatnik Center for Drug Discovery
George S. Wise Faculty of Life Sciences
Tel Aviv University
Tel Aviv 69978, Israel

A. Lampel
Center for Nanoscience and Nanotechnology
Tel Aviv University
Tel Aviv 69978, Israel

A. Lampel
Sagol Center for Regenerative Biotechnology
Tel Aviv University
Tel Aviv 69978, Israel

A. Lampel
Center for the Physics and Chemistry of Living Systems
Tel Aviv University
Tel Aviv 69978, Israel

Peptides are attractive building blocks for construction of functional biomaterials,[18–20] including those composed of liquid assemblies,[21–27] as their side-chain groups provide a diverse set of simple chemical functionalities that collectively constitute a rich and versatile chemical space.[28] Unlike proteins, peptide composition, even at the single-amino acid level,[29] directly dictates the supramolecular structure and material properties,[18] thereby enabling sequence-structure and structure-function relationships to be established. Here, we focused on viral factories formed by measles virus as a model system, and searched for prevalent amino acids in the disordered region (P loop) of the phosphoprotein (P protein), one of the two main building blocks of measles viral factories.[3–5] The designed LLPS-promoting peptide, which contains prevalent amino acids from the P protein P loop, efficiently forms liquid droplets upon complexation with RNA. We showed that the material properties of the compartments can be tuned by simple changes to the peptide sequence, using systematic alanine (Ala) scanning analysis and construction of 14 sequence variants. We leveraged these findings to spatiotemporally regulate the dynamics of the compartments and their ability to encapsulate and release payloads. Specifically, we developed compartments that change their material properties by light-triggered changes to the chemical composition of the peptide building block. Our results show that the material properties of peptide/RNA liquid assemblies can be regulated by tuning peptide composition, and that these changes can be leveraged to readily regulate payload release from individual compartments in spatially and temporally controlled manner.

2. Results and Discussion

We utilized a minimalistic approach to design open liquid compartments inspired by the measles viral factories that are formed by complexation between RNA, the measles virus P protein (**Figure 1**), and other viral proteins.[3,5,29] The 14-mer viral-factory-inspired peptide (VFP-1) LGKSGRLPGKSGRV contains prevalent amino acids from the P loop of the P protein (Figure S1, Supporting Information), including leucine (Leu), glycine (Gly), proline (Pro), serine (Ser) and valine (Val). We also incorporated two arginines (Arg) and two lysines (Lys) within the peptide sequence, which are found in the P loop at a prevalence of 7% and 11%, respectively. We hypothesized that Gly will induce flexibility in the disordered peptide chain, which is key for LLPS,[30–32] while Arg and Lys can promote electrostatic or cation–π interaction with RNA,[33] and the non-polar amino acids (Val, Leu) will promote hydrophobic interactions between the peptide molecules. Following peptide synthesis and purification (Figure S2, Supporting Information), we studied the LLPS propensity of the peptide and its ability to form liquid compartments by complex coacervation with RNA, using poly(uridylic acid) (poly-U) as an RNA model system. VFP-1 forms liquid droplets in the presence of poly-U at low $\times 10^{-3}$ M peptide concentrations (**Figure 2**a, Figure S3, Supporting Information). Circular dichroism (CD) analysis showed that the peptide is disordered and does not adopt a secondary structure in the presence of poly-U (Figure S4, Supporting Information). We were able to tune droplet diameter by varying the concentration of poly-U, the bulkier building block of the two. Dynamic light scattering (DLS) analysis of droplet size distribution accompanied by optical microscopy imaging show that droplet diameter increases linearly by increasing the concentration of poly-U from 0.1 mg mL^{-1} to 0.3 mg mL^{-1} (Figure 2b). Further increase in poly-U concentration to 0.5 mg mL^{-1} results in formation of droplets with a wide size distribution ranging from 300 to 1000 nm. By contrast, varying VFP-1 concentration while keeping a constant poly-U concentration has a minor effect on droplet diameter (Figure 2c). Since viral factories sequester both structured and unstructured RNA, we examined whether VFP-1 can undergo LLPS with tRNA, as a model for structured RNA. We found that VFP-1/tRNA LLPS is temperature-dependent, as no droplets are formed up to 40 °C. Droplet abundancy increases with increasing temperatures between 40 and 60 °C (Figure S5, Supporting Information). These results suggest that VFP-1/RNA LLPS is mediated by complexation of the peptide with partially, or fully, disordered RNA and that unfolding of the tRNA is critical for droplet formation.

To get a better understanding of the role of each amino acid of VFP-1 in LLPS and droplet formation, we performed alanine (Ala) scanning. Each of the amino acids of VFP-1 was substituted with Ala, resulting in 14 sequence variants (Table S1, Supporting Information). Following peptide synthesis and purification, we analyzed the LLPS propensity of each peptide at varying poly-U concentrations (0.3, 0.5, 1 mg mL^{-1}) (**Figure 3**a), where increasing the poly-U concentration increases sample turbidity. Substituting each of the basic amino acids with Ala (K3A, R6A, K10A, or R13A) completely arrested LLPS and droplet formation (Figure 3a, Figure S6, Supporting Information). This finding correlates with previous work which suggests that peptide/RNA complex coacervation is mainly driven by electrostatic interactions.[21,23] While all Ala substitutions of non-basic amino acids result in droplet formation, substituting specific amino acids with Ala affects LLPS propensity. Specifically, Pro/Ala substitution (P8A) increases sample turbidity and droplet diameter while milder increase in turbidity is observed for Ser/Ala substitution at position 11 (S11A) and Val/Ala substitution (V14A) (Figure 3a Figure S6, Supporting Information).

Next, we studied how these specific changes to the peptide sequence affect the material properties of the droplets. For this, we performed fluorescence recovery after photobleaching (FRAP) analysis of VFP-1, G5A, P8A, S11A, and V14A using laser scanning confocal microscopy (for details see Experimental Section). Droplets formed by VFP-1/poly-U are highly dynamic, with 96% recovery of fluorescence after photobleaching (Figure 3b,c) and a $t_{1/2}$ of 0.7 s (Figure 3d), two orders of magnitude higher than the reported recovery for measles viral factories formed in cells and in vitro.[3,4] A decrease in droplet diffusion is observed for P8A, S11A, and V14A (Figure 3b–d, Table S2, Supporting Information), with more than fourfold increase in $t_{1/2}$ observed for V14A compared with VFP-1 (Figure 3d), while no significant difference in droplet dynamics is observed for G5A. These results suggest that droplet dynamics can be tuned by simple changes to the peptide chemical composition.

Based on these findings, we hypothesized that the material properties of the compartments can be temporally modulated by controlling peptide charge and polarity using external stimulus. For this, we side-chain-protected Lys at position

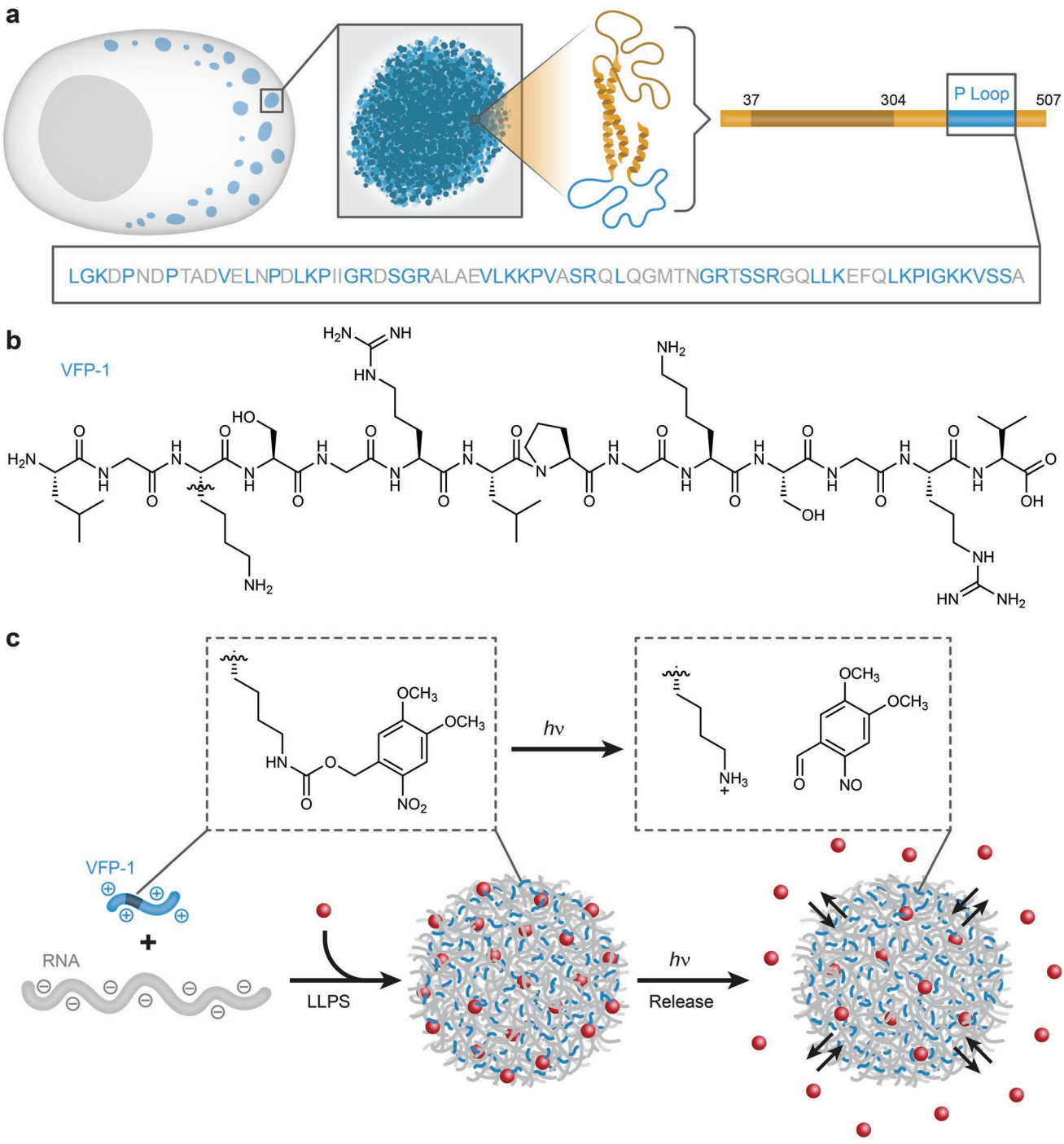

Figure 1. Design of viral-factory-inspired compartments. a) Schematic illustration of viral factories formed in the host cell including measles virus phosphoprotein (P protein, in yellow and blue). The disordered P loop region of the P protein is indicated (blue). b) Chemical structure of viral-factory-inspired peptide (VFP-1) containing amino acids which are prevalent in the P protein P loop. c) Top: Chemical structure of Lys (position 3) side chain protected by the photocleavable group Nvoc. The Nvoc group is cleaved from Lys side chain following UV irradiation. Bottom: Schematics of liquid compartments formed by LLPS of Nvoc-VFP-1 peptide and RNA (poly-U), encapsulating a fluorescent payload (red). Irradiation of the compartment leads to increased dynamics and payload release.

3 with the photocleavable group *o*-nitroveratryloxycarbonyl (Nvoc) (Figure 1c). Considering that Ala substitution of Lys at this position completely arrested LLPS, we expected that Nvoc conjugation to Lys will significantly affect LLPS propensity and droplet dynamics. Specifically, we expected that this hydrophobic and aromatic group will promote hydrophobic or π–π interactions between the peptide molecules or between the peptide and RNA, and as a result, decrease droplet dynamics.

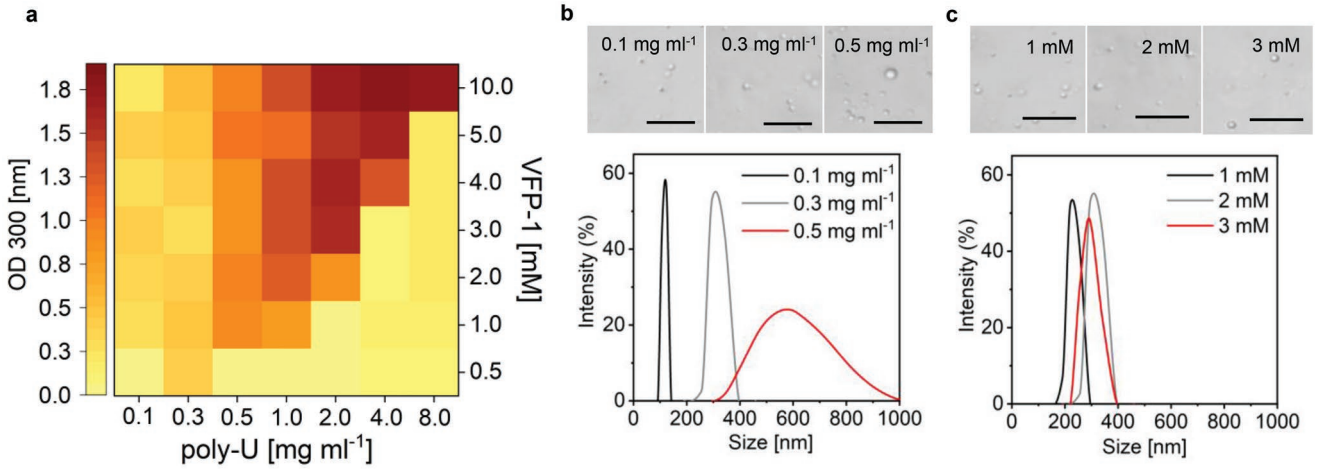

Figure 2. Viral-factory-inspired compartments formed by peptide/RNA LLPS. a) Phase diagram heatmap showing VFP-1/poly-U LLPS propensity at pH 7.5 as a function of peptide/RNA concentration measured by turbidity. b,c) Optical microscopy (top) and DLS (bottom) analyses of droplet size as a function of RNA (b) or peptide (c) concentration: b) droplets formed by LLPS of 2×10^{-3} M VFP-1 at varying poly-U concentrations; c) droplets formed by 0.3 mg mL^{-1} poly-U with VFP-1 at varying concentrations. Scale bars = 20 µm.

Thus, light-triggered removal of the Nvoc group from compartments that are formed by the Lys-protected peptide (Nvoc-VFP-1) will increase peptide polarity, reduce peptide–peptide contacts, promote electrostatic interactions between the peptide and poly-U and increase droplet dynamics, as reflected in the diffusion and mobility of peptide/RNA. Following synthesis

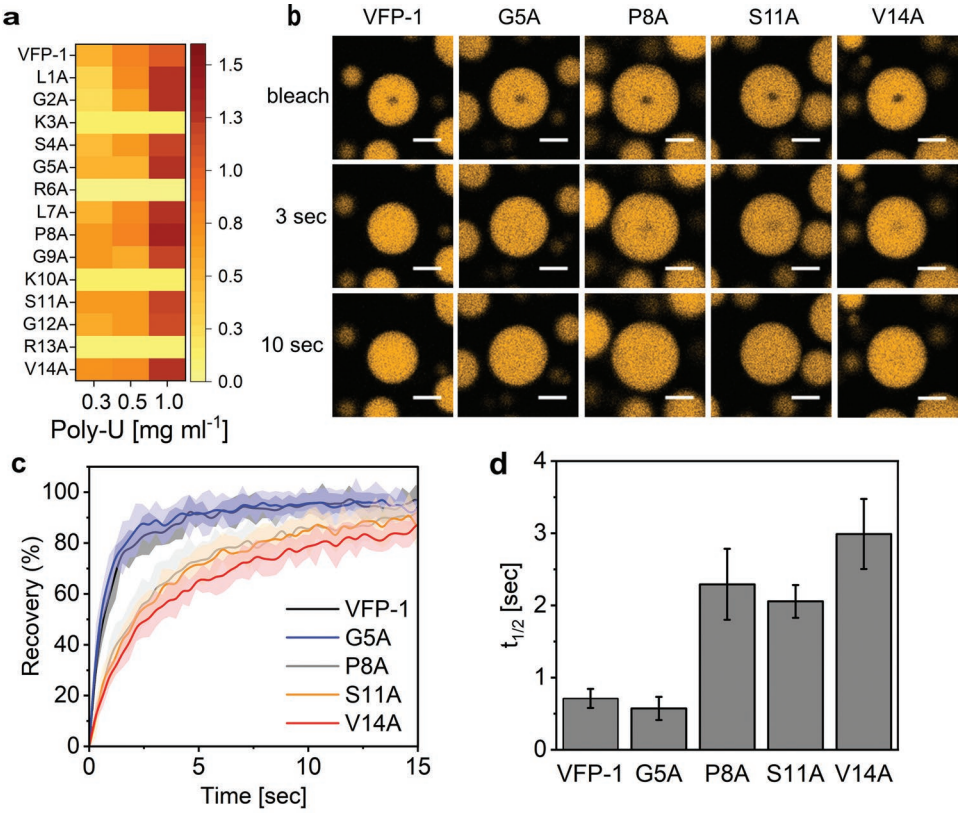

Figure 3. Electrostatic interactions are the main driving force of compartments formation as suggested by Ala scanning. a) Phase diagram heat map showing the effect of Ala substitution of each amino acid within VFP-1 (3×10^{-3} M) on LLPS with poly-U at varying concentrations (0.3–1 mg mL^{-1}). b–d) Fluorescence recovery after photobleaching (FRAP) analysis of VFP-1 sequence variants using laser scanning confocal microscopy with VFP-1-poly-U in the presence of Cy3-oligo-A. b) Confocal microscopy images of VFP-1 and its sequence variants (G5A, P8A, S11A, V14A) at varying time points after photobleaching containing droplets formed by 3×10^{-3} M peptide with 1 mg mL^{-1} poly-U. Scale bars = 5 µm. c) Recovery of plots as a function of time after photobleaching. d) Apparent $t_{1/2}$ calculated from recovery plots. Values represent average of $n = 9$, standard deviation is presented.

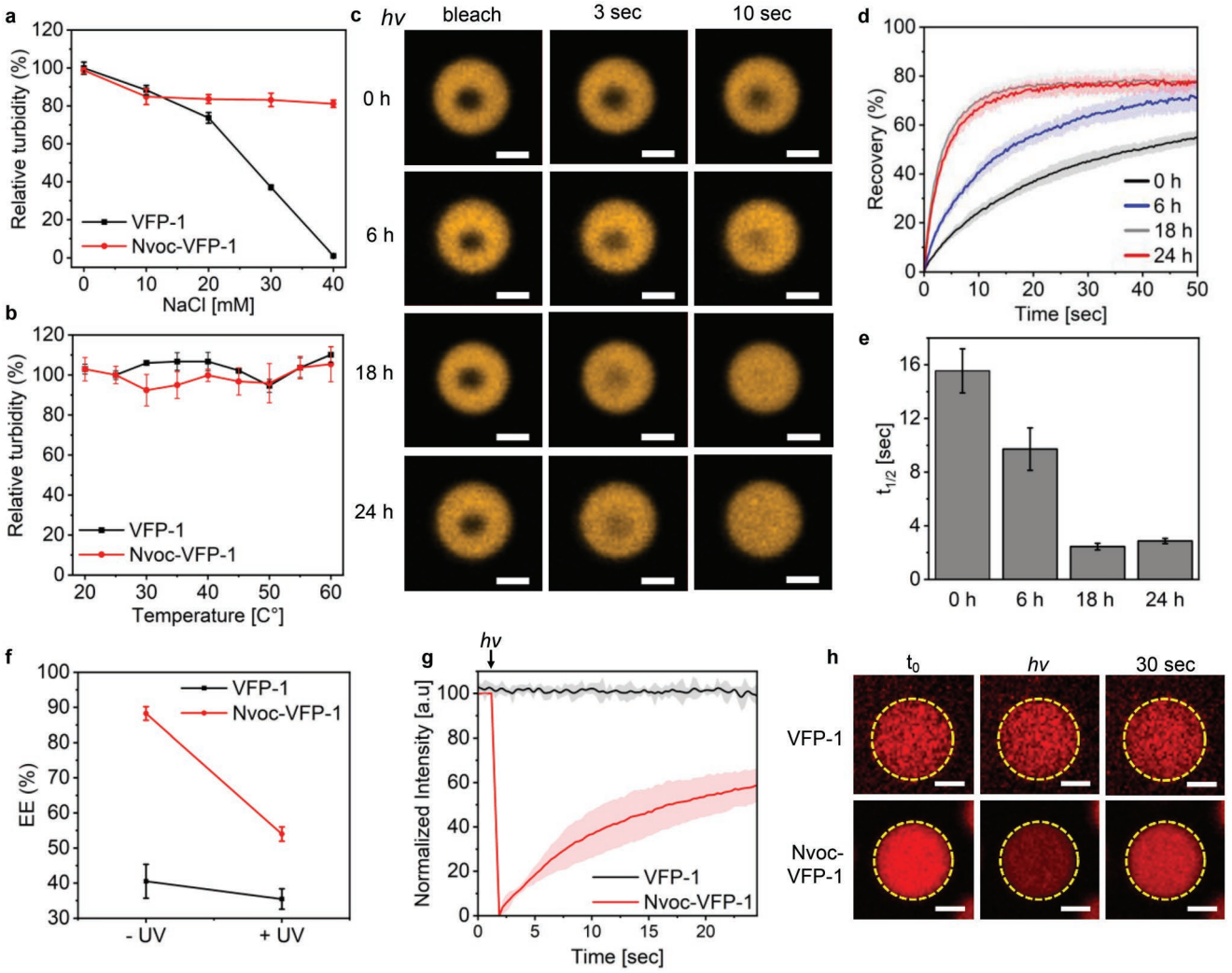

Figure 4. Light-controlled modulation of compartments' material properties and payload release. a,b) Effect of increasing NaCl concentration (a) or temperature (b) on formation of VFP-1 and Nvoc-VFP-1 droplets measured by turbidity assay. c–e) FRAP analysis of compartments formed by Nvoc-VFP-1/poly-U at varying irradiation times showing tunable diffusivity: c) confocal microscopy images of Nvoc-VFP-1 after varying irradiation time (0, 6, 18, 24 h) 3, 10 s, and immediately after photobleaching; d) recovery plots extracted from the FRAP analysis, and e) calculated $t_{1/2}$. Values represent average of $n = 10$, standard deviation is presented. Scale bars = 2 µm. f) Encapsulation efficiency (EE) analysis of rhodamine B (RhB) in compartments formed by either VFP-1 or Nvoc-VFP-1 as a function of UV irradiation ($t = 24$ h). g,h) RhB release from VFP-1 and Nvoc-VFP-1 compartments following selective excitation ($\lambda_{ex} = 405$ nm) of individual droplets using laser scanning confocal microscopy. g) RhB fluorescent signal in droplets ($\lambda_{ex} = 561$ nm) before and after irradiation of individual droplets. Values represent average of $n = 5$, standard deviation is presented. h) Confocal microscopy images of RhB release from droplets following irradiation. Scale bars = 2 µm.

and purification of Nvoc-VFP-1 (Figure S7, Supporting Information), we first analyzed the effect of temperature and salt on formation of liquid droplets by VFP-1/RNA compared to Nvoc-VFP-1/RNA. Addition of NaCl at concentrations ranging between 10 and 40 × 10^{-3} M results in concentration-dependent inhibition of VFP-1/RNA LLPS, where sample turbidity gradually decreases at increasing NaCl concentrations and a complete arrest of droplet formation is observed at 40 × 10^{-3} M NaCl (**Figure 4**a). In contrast, salt has a minor effect on Nvoc-VFP-1/RNA droplet formation, as 40 × 10^{-3} M NaCl results in only 17% decrease in sample turbidity and no change in droplet abundance is observed by optical microscopy (Figure S8a, Supporting Information). These results correlate with the findings from the Ala scanning analysis, further suggesting that the main driving force of VFP-1/RNA LLPS is electrostatic interactions, whereas Nvoc-VFP-1/RNA droplets are formed by additional modes of interaction such as π–π, cation–π, or hydrophobic interactions. Increasing the temperature of the sample has a negligible effect on droplet formation by both peptides (Figure 4b, Figure S8b, Supporting Information), ruling out contribution of hydrogen bonding in LLPS of either VFP-1/RNA or Nvoc-VFP-1/RNA.

We analyzed Nvoc cleavage from the peptide as a function of UV irradiation ($\lambda = 365$ nm) using HPLC (Figure S9, Supporting Information). This analysis confirmed that the Nvoc group is ≈95% cleaved from the peptide after irradiation for 24 h. Next, we analyzed how compartment irradiation affects the material properties of individual droplets using FRAP analysis, where

we measured droplets following varying irradiation times. This analysis shows that the total recovery of fluorescent signal after photobleaching depends on the irradiation time, where 6 h of irradiation increases the total recovery by 16% compared with unirradiated compartments (Figure 4c–e). Moreover, controlling the irradiation time results in tunable diffusion coefficient (D) and $t_{1/2}$ (Figure 4d,e, Table S3, Supporting Information) with a greater than sixfold decrease in $t_{1/2}$ following irradiation for 18 h (Figure 4e). These findings suggest that increasing droplet polarity by cleavage of the hydrophobic aromatic Nvoc group from the peptide building block increases droplet dynamics. Thus, the material properties of compartments can be temporally regulated by light-controlled changes to the chemical composition of the peptide building block.

We sought to investigate whether the temporal control over the peptide chemical composition and in turn droplet dynamics can be leveraged to regulate payload release from the compartments. For this, we first analyzed the encapsulation of fluorescent payload from the compartments following irradiation using Cy5 and rhodamine B (RhB). The calculated RhB encapsulation efficiency (EE%) of compartments formed by Nvoc-VFP-1 is 88% compared to 40% of VFP-1 compartments. This suggests that the Nvoc group promotes RhB encapsulation either by direct binding through hydrophobic or aromatic interactions, or indirectly, by inducing an overall hydrophobic microenvironment within the condensate which facilitates the recruitment of the dye. Following irradiation of the Nvoc-VFP-1 compartments, the EE of RhB decreases by 40% (Figure 4f). In contrast, irradiation of VFP-1 compartments has no significant effect on the EE of RhB. These results suggest that the encapsulation of RhB can be temporally controlled. By studying an additional fluorescent payload system using Cy5, we found similar trends, yet, the EE% of Cy5 by Nvoc-VFP-1 compartments (96%) is significantly higher than that of RhB (Figure S10a, Supporting Information), and the decrease in the EE after irradiation was much lower (6%, Figure S8a, Supporting Information). The major difference between the EE of RhB and Cy5 implies that the latter is not mediated by hydrophobic or aromatic interactions but rather by other modes, that is, electrostatic interactions with the basic side chain of the peptide.

Next, we performed a spatiotemporal analysis of RhB and Cy5 partitioning and release from droplets using confocal microscopy. Individual droplets formed by Nvoc-VFP-1 or VFP-1 were selectively excited using λ_{ex} = 405 nm laser. Excitation at this wavelength is expected to induce Nvoc cleavage but does not lead to photobleaching of RhB nor Cy5, as confirmed by analyzing the fluorescent signal of the dyes in VFP-1 droplets before and after irradiation (Figure 4g, Figure S10b, Supporting Information, Figure 4h, and Figure S10c, Supporting Information, top panel). Immediately after irradiating the Nvoc-VFP-1 compartments containing RhB, the fluorescent signal of the dye dropped drastically (Figure 4g,h). A partial increase in RhB signal is observed in the droplet over time, yet the finite recovery reaches ≈60% of the initial intensity, suggesting that RhB is released from the compartment. In contrast, no effect on the fluorescent signal of RhB in VFP-1 compartments was observed following irradiation. The finite fluorescent intensity of Cy5 in

Nvoc-VFP-1 droplets reach 88% following irradiation, which corresponds to the moderate change in EE of the dye in VFP-1 compartments following irradiation (Figure S10b,c, Supporting Information). In addition, we analyzed the partitioning and release of the enzyme tyrosinase and uridine-triphosphate (UTP) as model systems for enzymes and nucleotides, which are abundant in viral factories. Similar to Cy5 release, a sharp decrease in the fluorescence of Atto633-labeled tyrosinase and Atto647-labeled UTP is observed exclusively in Nvoc-VFP-1 droplets, but not in VFP-1 droplets, following irradiation (Figure S11, Supporting Information). In addition, a rapid fusion of neighboring droplets is observed only for Nvoc-VFP-1 and not for VFP-1 droplets, immediately after irradiation. These results suggest that we can spatially and selectively control the chemical composition of the compartments, and through light stimulus create a photochemical reaction that might allow real-time release of comparted molecules to the droplet surroundings.

3. Conclusions

We have developed dynamic peptide/RNA compartments that are inspired by disordered viral compartments. Using systematic studies of the peptide sequence we show that while the main driving force for LLPS and droplet formation is electrostatic interactions between the peptide and RNA, additional modes of interactions mediate LLPS, as specific Ala substitutions of non-basic amino acids affect the diffusivity of the compartments. By using a photocleavable side chain protecting group of the basic Lys, we develop compartmentalization system which can be regulated by light. While a light-triggered coacervation system was recently reported,[34] our results show that the dynamics and diffusion of compartments can be photomodulated and tuned over a wide range by increasing peptide polarity and charge. Importantly, we took this approach to the next level and leveraged the light-induced changes to the droplets' chemical composition to regulate the encapsulation and release of payloads from the compartments. The approach presented here holds promise for further development of stimuli-responsive reactors and delivery systems for targeted and personalized medical applications.

4. Experimental Section

Materials: Tris-HCl buffer was prepared with Trizma base (Sigma Aldrich) and adjusted to pH 7.5 with hydrochloric acid (HCl). Polyuridylic acid (polyU RNA) was purchased from Sigma Aldrich (P9528). 15 bases Cy3-oligoA were purchased from IDT. Pluronic-F127 for slide coating was purchased from Sigma Aldrich (P2443). Fmoc-L-Lys(Nvoc)-OH was purchased from Iris Biotech (FAA7230). Rhodamine B was purchased from Acros Organics (296570250). Cy5-COOH (MW 483.68 g mol^{-1}) was received from Prof. Roey Amir's lab, School of Chemistry, Faculty of Exact Sciences at Tel Aviv University. tRNA was purchased from Sigma Aldrich. Atto647-UTP was purchased from Jena Bioscience. Tyrosinase extracted from mushroom was purchased from Sigma Aldrich and labeled at amines using succinimidyl ester functionalized Atto633 labeling kit (Sigma).

Peptide Synthesis and Purification: All peptides were synthesized at the Blavatnik Center for Drug Discovery at Tel Aviv University, by solid phase peptide synthesis (SPPS) using Liberty Blue automated microwave peptide synthesizer on Fmoc-Val-Wang resin (0.311 meq g^{-1} substitution). Peptide crude purity was analyzed using LCMS (Waters Autopurification system, collaboration with Blavatnik center, see

details below). Crude was analyzed with analytical reverse-phase high-performance liquid chromatography (RP-HPLC, Thermo Fisher), a Dionex SD Ultimate 3000 UHPLC standard system equipped with a diode-array detection (DAD) Detector. Mobile phases were (A) H2O (0.1% trifluoroacetic acid; TFA) and (B) MeCN (0.1% TFA), stationary phase used was CS chromatography MultoHigh C18 column (250 mm × 4.6 mm, 5 µm particle size and 100 Å pore size, 5861272). Samples were then collected with a preparative RP-HPLC, similar to the analytical system with a Thermo-scientific fraction collector and a corresponding CS chromatography MultoHigh C18 column (250 mm × 10 mm, 5 µm particle size and 100 Å pore size, 510117225).

Alanine Scanning Peptide Synthesis and Purification: All 14 alanine scan peptides were synthesized in collaboration with Blavatnik center for drug discovery at Tel Aviv University. Peptide synthesis was performed as mentioned above, for V14A peptide Fmoc-Ala-Wang resin (0.380 meq g^{-1} substitution) was used. The peptides were analyzed on a Waters Autopurification system analytical module with a PDA detector equipped with a Waters Xselect Peptide CSH C18 column (5 µm, 4.6 mm × 100 mm). The Autopurification system was connected to a Waters SQD2 MS detector for structural determination. Separation was performed with a gradient elution of 0.1% FA in: i) H_2O and ii) MeCN with Xselect CSH C18 Prep Column (5 µm, 19 mm × 250 mm).

Peptide TFA Exchange: To remove TFA content that was left following peptide purification, two cycles of TFA exchange (with HCl) were performed. Purified peptide was dissolved in DDW to a final concentration of 2×10^{-3} M, then 1 M HCL was added at a final concentration of 7.5×10^{-3} M, after a few moments the samples were freeze-dried. After two cycles of TFA exchange the samples were tested in F-NMR for verification that no TFA was left. F-NMR spectra were collected in D_2O using a Bruker Advance III spectrometer at 400 MHz at the Department of Chemistry NMR Facility at Tel Aviv University.

LLPS Propensity Analysis and Phase Diagrams: Poly-U was dissolved in ultrapure water (19.5 mg mL^{-1}) and stored at −20 °C. 20×10^{-3} M VFP-1 stock was prepared in 10×10^{-3} M Tris buffer and adjusted to pH 7.5. Poly-U was added to peptide solution at varying concentrations to initiate LLPS. Turbidity was immediately visible upon poly-U addition. UV–vis absorbance spectra were taken using a Synergy H1 microplate reader, at λ = 300–700 nm after 30 s shaking. Phase diagrams were created based on turbidity measured using 384-well plate at $\lambda = 300$ nm. To analyze the effect of salt and temperature on LLPS, turbidity was measured at varying concentrations of NaCl ($10–40 \times 10^{-3}$ M) or varying temperatures between 20 and 60 °C using Synergy H1 microplate reader. Salt was added to samples of 2×10^{-3} M VFP-1 and 1 mg mL^{-1} poly-U or 1×10^{-3} M Nvoc-VFP-1 and 0.5 mg mL^{-1} poly-U, due to saturation of the Nvoc-VFP-1/poly-U turbidity signal at 2×10^{-3} M.

Optical Microscopy: Optical microscopy images were taken with inverted microscope (OPTIKA Microscopes Italy) with X-LED 8 W lamp and 60× objective using clear glass bottom 96-well plate for microscopy analysis. For optical microscopy analysis of droplet formation by VFP-1/tRNA, 1 mg mL^{-1} of tRNA was used. 50 µL Samples were analyzed following 2 min incubation at varying temperatures using an orbital mixing-heating incubator (Torrey Pines Scientific Inc).

Dynamic Light Scattering: DLS was performed using Malvern Zetasizer ZS instrument equipped with a 633 nm He–Ne laser and aligned for backscattering at 173°. Malvern software was used to analyze inverse Laplace transforms of the intensity autocorrelation functions using the non- 4 negatively constrained least squares algorithm to obtain multimodal size distribution data. Samples were prepared and pH-adjusted without poly-U, which was added to initiate LLPS immediately before DLS measurements. Each measurement was a mean of 10 measurements calculated by the Malvern software.

Confocal Microscopy: The fluorescence images were obtained using Zeiss Zen 900 confocal microscope with ×20/0.8 NA Plan- Apochromat air objective at 1 AU pinhole. All confocal samples were imaged on top of a Pluronic-F127-coated slide. Cy3 and rhodamine B images were taken with λ_{ex} = 561 nm laser, λ_{ex} = 640 nm laser for Cy5.

Fluorescence Recovery After Photobleaching: All FRAP samples were obtained using 2×10^{-3} M peptide, 1 mg mL^{-1} poly-U and 0.04×10^{-6} M Cy3-oligo-A in 10×10^{-3} M Tris buffer at pH 7.5. FRAP analysis was performed using Cy3-conjugated oligo-adenosine (Cy3-oligo-A, 15-mer)[21] (λ_{ex} = 561) with 15× crop magnification (128 × 128 pixels). Bleach area radius 0.5 µm, using 100% lasers. For Ala scanning FRAP analysis, the following lasers were used for photobleaching: λ_{ex} = 405, 488, 561, 640 nm. For Nvoc-VFP-1 FRAP analysis, the following lasers were used for photobleaching: λ_{ex} = 488, 561, and 640 nm, excluding λ_{ex} = 405 nm to avoid Nvoc photocleavage. Plot exponential fitting and recovery half-life were calculated using OriginLab. Final values were averaged from $n = 9$ (Figure 3) or $n = 10$ droplets (Figure 4). The apparent diffusion coefficient (D) of droplets formed by each of the peptides was calculated as:

$$D_{app} = \frac{r^2}{t} \quad (1)$$

where t is the recovery time obtained from the recovery plots and r is the radius of the photobleached area.

UV Irradiation of Nvoc-VFP-1: UV irradiation was performed using a UV-box equipped with a $\lambda = 365$ nm UV lamp (VILBER-LOURMAT, 6 W). Samples were prepared in 1 mL glass vials and placed inside the box.

Nvoc-VFP-1 Cleavage Analysis Using HPLC: Nvoc-VFP-1 was irradiated for 4 h, 8 h, 12 h, and 24 h. Following each time point, samples were analyzed using analytical RP-HPLC detailed above and % of cleavage was calculated from chromatogram peak integrals using Chromeleon software tools.

Dye Encapsulation Efficiency Analysis: Nvoc-VFP-1/VFP-1 were dissolved in 10 mM Tris buffer (pH 7.5, 2×10^{-3} M peptide) and irradiated for 24 h or placed in darkness for 24 h. After 24 h, poly-U (1 mg mL^{-1}) and dye (rhodamine B or Cy5, 5×10^{-6} M) were added. Droplet samples were centrifuged (1000 RPM, 10 min) and supernatants were collected for absorbance spectra measurements in triplicates (using 384-well plate). Background measurements of samples without dye and only buffer samples were subtracted from sample measurements. EE% was calculated as:

$$\text{EE\%} = \frac{\text{Total dye concentration} - \text{Supernatant dye concentration}}{\text{Total dye concentration}} \times 100 \quad (2)$$

Supernatant dye concentration was calculated from calibration curves for each dye (rhodamine B or Cy5) prepared using varying dye concentrations (20, 15, 10, 5, 1, 0.5×10^{-6} M).

Dye Encapsulation in Individual Droplets: Rhodamine B/Cy5 (0.05×10^{-6} M), Atto633-tyrosinse (0.7×10^{-6} M), or Atto647-UTP (1×10^{-6} M) were added to droplets formed by Nvoc-VFP-1/poly-U or VFP-1/poly-U (using 2×10^{-3} M peptide and 1 mg mL^{-1} poly-U, respectively). Droplets encapsulating dye were irradiated using the λ_{ex} = 405 nm laser, and the fluorescent signal of the dye in the droplets was monitored before and immediately after irradiation using λ_{ex} = 561/640 nm laser (561 nm for rhodamine B and 640 nm for Cy5, Atto633-tyrosinase, and Atto647-UTP). Normalized fluorescence values were obtained by using the average minimal intensity of Nvoc-VFP-1 droplets ($n = 5$ for RhB/Cy5, $n = 8$ for Atto633-tyrosinase/Atto647-UTP).

Supporting Information

Supporting Information is available from the Wiley Online Library or from the author.

Acknowledgements

The authors thank the Blavatnik Center for Drug Discovery for the support in peptide synthesis. Specifically, the authors thank B. Redko for help with Ala scanning peptide synthesis and purification. This research was supported by the Israel Science Foundation (Grant No. 2589/21).

The authors thank Prof. R. J. Amir from Tel Aviv University for providing Cy5, Mr. E. Silberman, and Mr. Adi Ben-Yaakov for technical assistance with rheology studies, Prof. E. Bacharach for advice on viral systems, and Dr. R. Fischer from the Advanced Science Research Center of the City University of New York (CUNY) for advice on FRAP analysis.

Conflict of Interest

The authors declare no conflict of interest.

Data Availability Statement

The data that support the findings of this study are available in the supplementary material of this article.

Keywords

coacervates, liquid droplets, liquid–liquid phase separation, membraneless organelles, peptides, viral factories

Received: July 13, 2022
Revised: September 15, 2022
Published online:

[1] J. Nikolic, R. L. Bars, Z. Lama, N. Scrima, C. Lagaudrière-Gesbert, Y. Gaudin, D. Blondel, *Nat. Commun.* **2017**, *8*, 58.
[2] Q. Nevers, A. A. Albertini, C. Lagaudrière-Gesbert, Y. Gaudin, *Biochim. Biophys. Acta, Mol. Cell Res.* **2020**, *1867*, 118831.
[3] Y. Zhou, J. M. Su, C. E. Samuel, D. Ma, *J. Virol.* **2019**, *93*, e00948.
[4] S. Guseva, S. Milles, M. R. Jensen, N. Salvi, J. P. Kleman, D. Maurin, R. W. H. Ruigrok, M. Blackledge, *Sci. Adv.* **2020**, *6*, eaaz7095.
[5] S. Guseva, S. Milles, M. Blackledge, R. W. H. Ruigrok, *Front. Microbiol.* **2019**, *10*, 1832.
[6] A. Savastano, A. Ibáñez de Opakua, M. Rankovic, M. Zweckstetter, *Nat. Commun.* **2020**, *11*, 6041.
[7] T. M. Perdikari, A. C. Murthy, V. H. Ryan, S. Watters, M. T. Naik, N. L. Fawzi, *EMBO J.* **2020**, *39*, 106478.
[8] S. Alberti, A. A. Hyman, *Nat. Rev. Mol. Cell Biol.* **2021**, *22*, 196.
[9] D. Bracha, M. T. Walls, C. P. Brangwynne, *Nat. Biotechnol.* **2019**, *37*, 1435.
[10] S. F. Banani, H. O. Lee, A. A. Hyman, M. K. Rosen, *Nat. Rev. Mol. Cell Biol.* **2017**, *18*, 285.
[11] V. Verdile, E. De Paola, M. P. Paronetto, *Front. Genet.* **2019**, *10*, 173.
[12] J. M. Su, M. Z. Wilson, C. E. Samuel, D. Ma, *Viruses* **2021**, *13*, 126.
[13] S. Brocca, R. Grandori, S. Longhi, V. Uversky, *Int. J. Mol. Sci.* **2020**, *21*, 9045.
[14] S. Alberti, D. Dormann, *Annu. Rev. Genet.* **2019**, *53*, 171.
[15] S. Roberts, T. S. Harmon, J. L. Schaal, V. Miao, K. (J.) Li, A. Hunt, Y. Wen, T. G. Oas, J. H. Collier, R. V. Pappu, A. Chilkoti, *Nat. Mater.* **2018**, *17*, 1154.
[16] K. Deepankumar, Q. Guo, H. Mohanram, J. Lim, Y. Mu, K. Pervushin, J. Yu, A. Miserez, K. Deepankumar, Q. Guo, J. Yu, A. Miserez, H. Mohanram, J. Lim, Y. Mu, K. Pervushin, *Adv. Mater.* **2022**, *34*, 2103828.
[17] L. Faltova, A. M. Küffner, M. Hondele, K. Weis, P. Arosio, *ACS Nano* **2018**, *12*, 9991.
[18] M. J. Webber, E. A. Appel, E. W. Meijer, R. Langer, *Nat. Mater.* **2016**, *15*, 13.
[19] H. S. Azevedo, A. Mata, *Biomater. Biosyst.* **2022**, *6*, 100039.
[20] A. Lampel, *Chem* **2020**, *6*, 1222.
[21] W. M. Aumiller, C. D. Keating, *Nat. Chem.* **2016**, *8*, 129.
[22] M. Abbas, W. P. Lipiński, J. Wang, E. Spruijt, *Chem. Soc. Rev.* **2021**, *50*, 3690.
[23] C. Donau, F. Späth, M. Sosson, B. A. K. Kriebisch, F. Schnitter, M. Tena-Solsona, H. S. Kang, E. Salibi, M. Sattler, H. Mutschler, J. Boekhoven, *Nat. Commun.* **2020**, *11*, 5167.
[24] B. Gabryelczyk, H. Cai, X. Shi, Y. Sun, P. J. M. Swinkels, S. Salentinig, K. Pervushin, A. Miserez, *Nat. Commun.* **2019**, *10*, 1.
[25] M. Abbas, W. P. Lipiński, K. K. Nakashima, W. T. S. Huck, E. Spruijt, *Nat. Chem.* **2021**, *13*, 1046.
[26] Y. Shen, F. S. Ruggeri, D. Vigolo, A. Kamada, S. Qamar, A. Levin, C. Iserman, S. Alberti, P. S. George-Hyslop, T. P. J. Knowles, *Nat. Nanotechnol.* **2020**, *15*, 841.
[27] J. Lim, A. Kumar, K. Low, C. S. Verma, Y. Mu, A. Miserez, K. Pervushin, *J. Phys. Chem. B* **2021**, *125*, 6776.
[28] A. Lampel, R. V. Ulijn, T. Tuttle, *Chem. Soc. Rev.* **2018**, *47*, 3737.
[29] A. Lampel, S. A. McPhee, H. A. Park, G. G. Scott, S. Humagain, D. R. Hekstra, B. Yoo, P. W. J. M. Frederix, T. De Li, R. R. Abzalimov, S. G. Greenbaum, T. Tuttle, C. Hu, C. J. Bettinger, R. V. Ulijn, *Science* **2017**, *356*, 1064.
[30] T. S. Harmon, A. S. Holehouse, M. K. Rosen, R. V. Pappu, *Elife* **2017**, *6*, e30294.
[31] A. E. Baruch Leshem, S. Sloan-Dennison, T. Massarano, S. Ben-David, D. Graham, K. Faulds, H. E. Gottlieb, J. H. Chill, A. Lampel, *ChemRxiv* **2022**, https://doi.org/10.26434/CHEMRXIV-2022-013K3.
[32] K. L. Saar, A. S. Morgunov, R. Qi, W. E. Arter, G. Krainer, A. A. Lee, T. P. J. Knowles, *Proc. Natl. Acad. Sci. USA* **2021**, *118*, e2019053118.
[33] R. S. Fisher, S. Elbaum-Garfinkle, *Nat. Commun.* **2020**, *11*, 4628.
[34] N. Gao, C. Xu, Z. Yin, M. Li, S. Mann, *J. Am. Chem. Soc.* **2022**, *144*, 3855.